HAL
open science

Benzothioxanthene Dicarboximide as a Tuneable Electrogenerated Chemiluminescence Dye

Alice L Dauphin, José María Andrés Castán, Jing Yu, Philippe Blanchard, Neso Sojic, Hyun S Ahn, Bright Walker, Clément Cabanetos, Laurent Bouffier

To cite this version:

Alice L Dauphin, José María Andrés Castán, Jing Yu, Philippe Blanchard, Neso Sojic, et al.. Benzothioxanthene Dicarboximide as a Tuneable Electrogenerated Chemiluminescence Dye. ChemElectroChem, 2022, 9 (24), 10.1002/celc.202200967 . hal-04273981

HAL Id: hal-04273981

https://hal.science/hal-04273981v1

Submitted on 8 Nov 2023

HAL is a multi-disciplinary open access archive for the deposit and dissemination of scientific research documents, whether they are published or not. The documents may come from teaching and research institutions in France or abroad, or from public or private research centers.

L'archive ouverte pluridisciplinaire **HAL**, est destinée au dépôt et à la diffusion de documents scientifiques de niveau recherche, publiés ou non, émanant des établissements d'enseignement et de recherche français ou étrangers, des laboratoires publics ou privés.

Benzothioxanthene dicarboximide core as a tuneable electro-generated chemiluminescence dye

Alice L. Dauphin,[a] José María Andrés Castán,[b] Jing Yu,[a] Philippe Blanchard,[b] Neso Sojic,[a] Hyun S. Ahn,[c] Bright Walker,[d] Clément Cabanetos,[b,e] and Laurent Bouffier*[a]

Abstract: Overlooked for years, the promising benzothioxanthene dicarboximide (BTXI) structure is nonetheless known to be an excellent fluorophore. As a further step towards the exploration of this rylene structure, the generation of electrochemiluminescence (ECL) in acetonitrile solutions is investigated herein as well as its direct comparison with a diphenylamine (DPA) derivative. Electrochemical characterization shows that the bare BTXI can be reversibly reduced or oxidized, characteristics which suggest the possibility that the electrogenerated reactive species can be exploited in the context of ECL. As a result, the BTXI moiety was found to be ECL-active in both annihilation and co-reactant mechanisms. Tri-*n*-propylamine (TPA) and benzoyl peroxide (BPO) were selected as sacrificial co-reactants for promoting ECL. An ECL efficiency of 13% (BTXI) and 6% (BTXI-DPA) compared to that of $Ru(bpy)_3^{2+}$ was found when using TPA in oxidative ECL. Moreover, the ECL efficiency increased to 75% and 55% of $Ru(bpy)_3^{2+}$ with BPO (i.e. reductive ECL) for BTXI and BTXI-DPA, respectively. These results can be understood by calculating the free enthalpy of the redox reactions associated with each ECL pathway. Although the BTXI-DPA red emitter exhibits more suitable thermodynamic properties, the BTXI green emitter is nonetheless more effective in combination with a co-reactant due to a much larger photoluminescence quantum yield. The ECL spectra of the two molecules are compared to their photoluminescence spectra, revealing the involvement of the same excited states in the two different photoemission processes. In turn, the chemical engineering of BTXI is shown to be an effective platform for achieving tuneable ECL generation.

Introduction

Electrogenerated chemiluminescence (ECL) has been investigated for decades as a special mode of chemiluminescence that is triggered by an electron transfer step at the electrochemical interface.[1-7] This process is initiated either by an oxidation or by a reduction occurring at the electrode surface. Such a heterogeneous electrochemical step generates reactive species that can further react in solution (*i.e.* homogenous steps) within the diffusion layer in order to populate the excited state of a given luminophore. Compared to photoluminescence (PL), ECL involves an electrochemical excitation and provides therefore photons without the necessity of photo-excitation. That is why ECL is very popular as a mode of transduction in many (bio)-sensors thanks to a very low background enabling high-sensitivity detection. Nowadays, ECL remains a very active field of research with a special focus on the development of new analytical strategies, the design of novel ECL-active luminophores, the use of ECL to study fundamental biochemical processes as well as the development of ECL-based electrochemical displays.[7-16] The inorganic ruthenium (II) complex bearing three bipyridines ($Ru(bpy)_3^{2+}$) is the most employed ECL luminophore since it exhibits an excellent compromise between electrochemical and photophysical properties enabling efficient ECL generation. However, many other inorganic or organometallic complexes based on ruthenium and/or iridium are still investigated in order to find new alternative dyes.[17-21] These inorganic luminophores offer a large molecular diversity, which is enabled by tuning the nature of the ligands surrounding the metal cation. Most of the time, their photophysical properties imply that a metal-to-ligand charge-transfer mechanism is responsible for the population of the excited state, which intrinsically limits the emission wavelength compared to a purely ligand-centred transition. In addition, the use of expensive metals, even at low concentrations can hinder a potential large-scale industrialization of such derivatives. On the other hand, organic molecules allow limitless possibilities in order to control the electronic properties and the resulting ECL capability.[22-26] One promising organic moiety, which can be prepared in only two steps on a multi-ton-scale is the highly fluorescent but overlooked benzothioxanthene (BTX) structure. BTX has never been investigated in the context of ECL, despite its great potential, and is thus evaluated herein. BTX is a well-known structure that has been employed for various applications. The fluorescent properties of BTX have been used to prepare ratiometric pH or halide sensors,[27-29] or to detect the presence of water content in organic solvents.[30] BTX was also highlighted as an efficient reporter for monitoring either chemical transformations or radical polymerizations.[31, 32] It was reported as a fluorescent label that can be incorporated inside polymer matrices or polymer particles such as latex or polystyrene.[33-36] Also, it can act as a fluorescent marker for DNA hybridization assays,[37] or to visualize a carbon nanotube dispersion by confocal laser scanning microscopy.[38] Finally, another key application takes advantage of BTX as a dopant when incorporated into electroluminescent devices such as organic solar cells or organic light-emitting diodes.[39-43] Very recently, benzothioxanthene dicarboximide (BTXI) was proposed as an imide-containing rylene chromophore. The functionalization of the pi-conjugated structure was demonstrated, enabling a high degree of control over the chemical reactivity through regioselective halogenation, nitration, dimerization, or cyanation reactions.[43-46] The establishment of a wide chemical library has been accomplished in an effort toward rationalizing and understanding the relationships between structure and photophysical properties, which can be finely tuned.[45, 47, 48]

In this work, we investigated for the first time the possibility of using BTXI as well as a diphenylamine (DPA) derivative (Scheme 1) to generate ECL in acetonitrile. The influence of this DPA group is anticipated to strongly modulate the corresponding ECL properties. Since ECL can be achieved following several mechanistic pathways, both the annihilation and the co-reactant strategies were thus investigated.

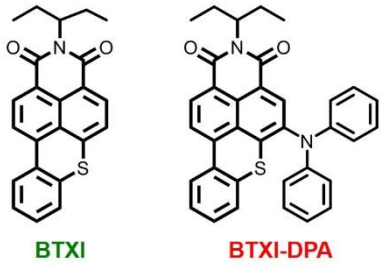

Scheme 1. Chemical structures of benzothioxanthene dicarboximide, abbreviated BTXI (left) and an analogue that is modified with a diphenylamine group BTXI-DPA (right).

Results and Discussion

The electrochemistry of the two ECL candidates was assessed by performing cyclic voltammetry (CV) in de-aerated CH_3CN solutions containing 1 mM of BTXI or BTXI-DPA and 0.1 M of $TBAPF_6$ as a supporting electrolyte. These CV traces were recorded using a glassy carbon (GC) working electrode and a silver wire pseudo-reference electrode at a scan rate of 0.1 V per second. As plotted in Figure 1a, BTXI can be reduced at –0.98 V *vs.* Ag while its oxidation takes place at 1.55 V *vs.* Ag (Table 1). Both mono-electronic processes were quasi-reversible with a peak separation of 0.12 and 0.08 V, respectively, and a ratio $\left|I_p^A/I_p^C\right|$ that was found to be slightly larger than unity (1.04 and 1.08, respectively). By comparison, BTXI-DPA is also reduced reversibly at –1.06 V *vs.* Ag with a peak-to-peak separation of 0.07 V and a current ratio value of 1.06 (Figure 1b and Table 1). On the other hand, the oxidation of BTXI-DPA that occurs at 1.35 V *vs.* Ag deviates from ideality. In fact, the forward scan features a unique oxidation peak (E_p^A = 1.39 V) while the backward scan reveals two successive reduction peaks, a main one at 1.31 V, immediately followed by another one at 1.17 V *vs.* Ag. The latter, observed from the very first backward scan can be assigned to a surface process occurring at the GC electrode since subsequent scanning also exhibited an additional pre-peak related to the oxidation. This means that a regular polishing of the electrode surface is mandatory due to a strong tendency of the electrogenerated species to self-adsorb at the surface of the working electrode. The exact nature of the species that does adsorb at the electrode surface is probably a dimer that is formed *in-situ* following the generation of the radical cation. Such a process being exclusively observed with BTXI-DPA suggests that the diphenylamine moiety is involved in the dimerization process, which has been previously reported.[49] Besides, both the oxidation and the reduction processes can be considered quasi-reversible for the two tested molecules. The ease of oxidation of BTXI-DPA compared to the parent BTXI structure can be attributed to the presence of the electron-donating DPA group that stabilizes the oxidized form. In the same way, the reduction occurring at a more negative potential value is also explained by the presence of the DPA group that confers a larger electron density and renders the reduction more difficult. Finally, we also collected CV of ferrocene (Figure S1) as an electrochemical standard under the same experimental conditions in order to verify the potential exhibited by the silver-wire pseudo-reference electrode. In that case, the Fc/Fc^+ redox couple displayed a formal potential value of 0.61 V *vs.* Ag.

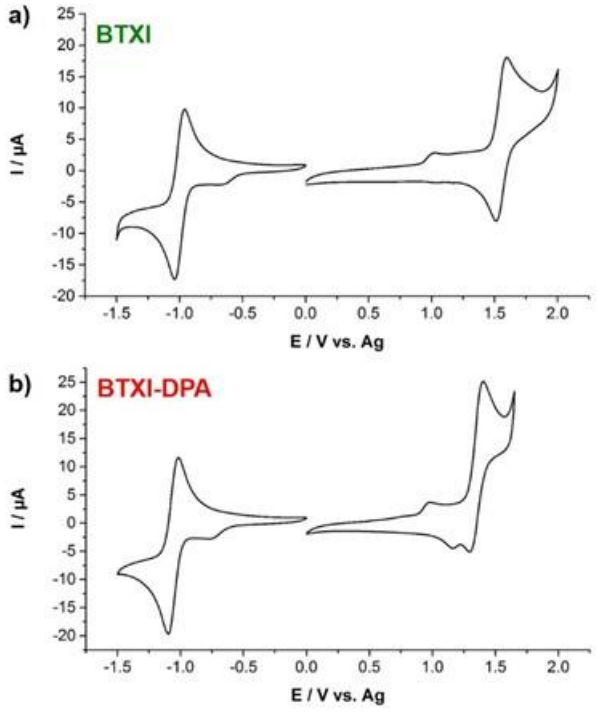

Figure 1. Cyclic voltammograms of 1 mM BTXI (a) and 1 mM BTXI-DPA (b) recorded at a glassy carbon (GC) electrode in CH_3CN with 0.1 M $TBAPF_6$ as supporting electrolyte. Scan rate 0.1 V s^{-1}. The potential is given *versus* a silver-wire pseudo-reference electrode.

Table 1. Electrochemical data

		E_p^A / V[a]	E_p^C / V[a]	$E_{½}$ / V[b]	ΔE_p / V[b]	$\lvert I_p^A/I_p^C \rvert$ [c]
BTXI	Oxid.	1.59	1.52	1.55	0.07	1.08
	Red.	–0.92	–1.04	–0.98	0.12	1.04
BTXI -DPA	Oxid.	1.39	1.31	1.35	0.08	1.40
	Red.	–1.02	–1.09	–1.06	0.07	1.06

[a] E_p^A and E_p^C are the anodic and cathodic peak potentials, respectively. [b] $E_{½}$ and ΔE_p are the formal potential and the difference between the two peak potentials, respectively. [c] $\lvert I_p^A/I_p^C \rvert$ is the absolute value of the ratio between the anodic and cathodic peak currents, respectively.

Table 2. Photoluminescence (PL) and Annihilation ECL data

	$\Delta E_{½}$ / V	λ_{PL} / nm[a]	ϕ_{PL}[a]	E_S / eV[b]	$\Delta G^0_{annih.}$ / eV[c]
BTXI	2.53	510	99%	2.43	–0.10
BTXI-DPA	2.41	600	33%	2.07	–0.34

[a] λ_{PL} and ϕ_{PL} are the photoluminescence wavelength and quantum yield, respectively. [b] E_S is the energy of the excited state. [c] $\Delta G^0_{annih.}$ is the free enthalpy of the annihilation reaction given in equation 3. It corresponds to the Gibbs free enthalpy without taking into account the entropy contribution (i.e. $\Delta G^0_{annih.} = E_S - \Delta E_{½}$).

The analysis of these electrochemical data allows the electrochemical gap between the oxidation and reduction of the BTXI-based dyes to be calculated. The corresponding $\boldsymbol{\Delta E_{½}}$ values were found to be 2.53 and 2.41 eV for BTXI and BTXI-DPA, respectively (Table 2). The PL spectra of the two molecules have previously been reported and featured large fluorescence bands centered at 510 and 600 nm, respectively.[45] These wavelengths can be used to estimate the energy of the excited state using the formula $\boldsymbol{E_S}$ (eV) = 1239.81 / $\boldsymbol{\lambda_{PL}}$ (nm). In both cases, the $\boldsymbol{E_S}$ values (Table 2) were found to be smaller than the $\boldsymbol{\Delta E_{½}}$ anticipating the possibility to generate ECL via the so-called annihilation pathway.[6] In this ECL mode, the potential applied to the working electrode is pulsed above the oxidation peak potential and below the reduction peak potential, respectively. These alternating pulses enable concomitant generation of the electro-oxidized and the electro-reduced forms in close vicinity of the electrode surface where these species can react with each other by homogeneous redox chemistry. This latter reaction is called an annihilation (between the oxidant and reductant, respectively) since the recombination regenerates the neutral species. The reactive oxidized and reduced species of the luminophore exergonically recombine with the concomitant emission of a photon and return to the neutral ground state of the luminophore. From Table 2, the corresponding free enthalpies of annihilation were found to be negative for BTXI and BTXI-DPA with a value of –0.10 eV and –0.34 eV, respectively meaning that these dyes are energetically capable of ECL by the so-called singlet route or S-route. It is noteworthy that this thermodynamic value does not correspond strictly to the Gibbs free energy since it is not corrected with the entropy contribution, which is usually negligible. One can find below a simplified mechanism comprising the sequence of steps for the annihilation pathway. The α coefficient reflects the competition between the excited state (kinetic product) *versus* ground state formation (thermodynamic product).

$$BTXI + e^- \rightarrow BTXI^{\bullet-} \quad \text{(reduction at the electrode)} \qquad (1)$$

$$BTXI - e^- \rightarrow BTXI^{\bullet+} \quad \text{(oxidation at the electrode)} \qquad (2)$$

$$BTXI^{\bullet-} + BTXI^{\bullet+} \rightarrow \alpha\, BTXI^* + (2 - \alpha)\, BTXI$$

$$\text{(annihilation reaction)} \qquad (3)$$

$$BTXI^* \rightarrow BTXI + h\nu \quad \text{(photon emission)} \qquad (4)$$

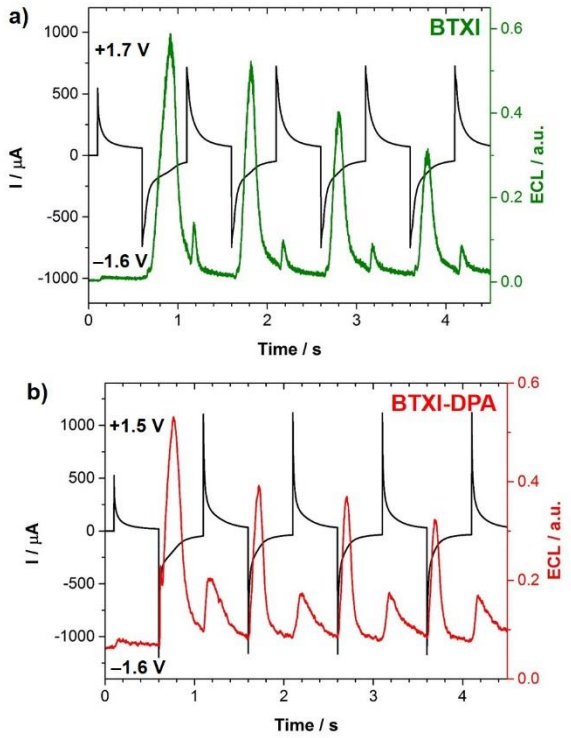

Figure 2. Chronoamperometric curves and ECL transients of 0.1 mM BTXI (a) and 0.1 mM BTXI-DPA (b) recorded in CH_3CN solution containing 0.1 M $TBAPF_6$. The potential is pulsed alternatively between the oxidation and reduction potential of the redox probes, respectively. Reference electrode: Silver wire. Pulses duration: 0.5 s.

The corresponding chronoamperometric curves and ECL transients were collected from a 0.1 mM solution of BTXI or BTXI-DPA in CH_3CN with 0.1 M $TBAPF_6$ (Figure 2). These ECL transients reveal that ECL emission is observed upon each individual pulsing except the first one since the concomitant presence of both the oxidized and reduced states is necessary prior to the annihilation reaction (eq. 3). A comparison between the ECL signals recorded for BTXI and diphenylamine-functionalized counterpart (BTXI-DPA) shows in both cases a similar maximum intensity. This might seem counterintuitive since the free enthalpy of annihilation is more favourable when the BTXI structure is conjugated with a DPA group. In fact, such a pure thermodynamic parameter does only reflect the propensity to populate the excited state. However, BTXI exhibits a very high quantum yield that is close to unity, meaning that this dye is particularly efficient in undergoing radiative de-excitation (Table 2). On the contrary, the quantum yield of BTXI-DPA is three times lower, resulting in less efficient photon emission during de-excitation of its singlet excited state. A comparison of the ECL amplitude obtained after the oxidative or reductive pulses is clearly asymmetric. For BTXI, the applied potential was pulsed between –1.6 V and +1.7 V *vs.* Ag pseudo-reference (Figure 2a) and in that case, the ratio between the ECL intensity collected after the negative pulse *versus* the positive pulse was larger than 4. This implies that the oxidized form is less stable compared to the reduced form and the former species is depleted in the vicinity of the electrode surface.

Comparable data were also collected at a higher frequency of 10 Hz (i.e. potential steps of 100 ms instead of 500 ms) in order to probe the stability of the corresponding electrogenerated species and revealed the same trend (data not shown). Also, a careful analysis of Figure 2a revealed a time delay between the applied potential pulse and the corresponding ECL transient for BTXI. This was only observed after the cathodic pulse and can therefore be safely assigned to the poor stability of $BTXI^{\bullet+}$. Such a delay was not observed with the DPA analogue or with BTXI when shortening the pulse duration to 0.1 sec. Also, the general trend is a regular decrease of the ECL signal upon repeated pulses, with 54% of the intensity remaining after the fourth cathodic pulse, compared to the first one. For BTXI-DPA, the experimental characterization is similar with a 40% loss of the ECL intensity after the fourth negative pulse. However, the oxidized form of BTXI-DPA appears more stable than the oxidized form of BTXI, with an average ECL peak ratio of ~ 2. It is noteworthy that a direct comparison between Figures 2a and 2b is possible since in both cases, the potential applied during the anodic pulse (that electro-generates the less stable species) was set at 150 mV above the oxidation potential ($\boldsymbol{E}_{½}$).

At that stage, we selected BTXI-DPA to study the influence of the applied potential on ECL generation. For that, we also collected another series of ECL transients by pulsing the applied potential between –1.6 V and +1.9 V *vs.* Ag pseudo-reference. The corresponding data are presented in Figure S2 and reveal a gain in ECL intensity recorded after the positive pulses with a ratio of ECL peaks of 1.2. It confirms that the ECL intensity can indeed be straightened by adjusting the driving force used for electrogenerating the reactive species involved in the molecular ECL mechanism.

Apart from the annihilation pathway, the other method to generate ECL is called the co-reactant pathway. In that case, the idea is not to apply potential pulses but to apply either an oxidation or a reduction potential continuously at the working electrode. Practically, the ECL-active dye is mixed in solution with a sacrificial co-reactant so that the latter will electrogenerate a highly reactive species. In that context, BTXI offers two possibilities since it can be either oxidized or reduced reversibly. The two most used co-reactants are tri-*n*-propylamine (TPA) to enable an "oxidative-reduction" or benzoyl peroxide (BPO) for the corresponding "reductive-oxidation". The generally accepted sequence of steps are the following for the ECL oxidation pathway with TPA are as follows:

$BTXI - e^- \rightarrow BTXI^{\bullet+}$ (oxidation of the dye) (2)

$TPA - e^- \rightarrow TPA^{\bullet+}$ (oxidation of the co-reactant) (5)

$TPA^{\bullet+} - H^+ \rightarrow TPA^{\bullet}$ (dissociation step) (6)

$BTXI^{\bullet+} + TPA^{\bullet} \rightarrow \beta\ BTXI^* + (1 - \beta)\ BTXI + Im^+$

(redox reaction) (7)

$BTXI^* \rightarrow BTXI + h\nu$ (photon emission) (4)

The oxidized form of the co-reactant, $TPA^{\bullet+}$, dissociates very quickly by losing a proton (eq. 6) in order to form $TPA^{\bullet}$, which is a strong reducer. In the literature, the corresponding potential has been reported to be −2.1 V *vs.* Fc/Fc^+.[19, 50, 51] Therefore, $TPA^{\bullet}$ undergoes a redox reaction with $BTXI^{\bullet+}$ to regenerate BTXI (one part (β) at the excited state and another part (1 – β) at the ground state) as well as an iminium species (Im^+). According to this mechanism, one can see that TPA is used as a stoichiometric sacrificial co-reactant while BTXI dye is regenerated to its ground state at the end of the sequence (eqs. 7 and 4).

In a similar pathway, the sequence of steps for the reduction pathway with BPO is as follows:

$BTXI + e^- \rightarrow BTXI^{\bullet-}$ (reduction of the dye) (1)

$BPO + e^- \rightarrow Ph\text{-}CO_2^{\bullet} + Ph\text{-}CO_2^-$ (reduction of the co-reactant concerted with a bond cleavage step) (8)

$BTXI^{\bullet-} + Ph\text{-}CO_2^{\bullet} \rightarrow \gamma\ BTXI^* + (1 - \gamma)\ BTXI + Ph\text{-}CO_2^-$

(redox reaction) (9)

$BTXI^* \rightarrow BTXI + h\nu$ (photon emission) (4)

Practically, the monoelectronic reduction of BPO that is supposed to yield a radical anion is coupled with the cleavage of the peroxyde O-O bond (eq.8). Therefore, this concerted electron transfer step forms one equivalent of carboxylate and one equivalent of the carboxyl radical, the latter being a strong oxidant. The corresponding potential has been discussed several times in the literature and the consensus is to use a value of +1.5 V *vs.* SCE.[51-54] Globally, BTXI is regenerated while a stoichiometric amount of BPO is consumed by forming two equivalents of benzoate. The feasibility of each ECL pathway can be estimated by calculating the free enthalpy of reactions 7 and 9, respectively. Hence, it was found that these $\boldsymbol{\Delta G^0_{ox-red}}$ or $\boldsymbol{\Delta G^0_{red-ox}}$ values are consitently negative, anticipating the possibility to obtain ECL using either dye and either sacrificial co-reactant (see Table 3 for details). In addition, the Gibbs free energy appears to be consistently more favorable for BTXI-DPA compared to BTXI with a gain of 0.16 eV with TPA and 0.44 eV with BPO, respectively.

Table 3. Co-reactant ECL data

		TPA co-reactant		BPO co-reactant	
	λ_{ECL}/ nm[a]	ϕ_{ECL}[a]	ΔG^0_{ox-red}/ eV[b]	ϕ_{ECL}[a]	ΔG^0_{red-ox}/ eV[b]
BTXI	520-530	13%	–0.61	75%	–0.20
BTXI -DPA	~615	6%	–0.77	55%	–0.64

[a] λ_{ECL} and ϕ_{ECL} are the electrogenerated chemiluminescence wavelength and yield, respectively. [b] ΔG^0_{ox-red} and ΔG^0_{red-ox} are the free enthalpy of the redox reaction involved in the co-reactant mechanism according to equations 7 and 10, respectively.

Experimentally, the ECL signal was recorded during the course of linear sweep voltammetry (LSV) on a GC working electrode positioned in front of a photodetector (see experimental details below). The CH_3CN solution contained 1 mM of BTXI or BTXI-DPA and either 100 mM of TPA or 10 mM of BPO in 0.1 M $TBAPF_6$. In the LSV trace of the dye associated with TPA (Figures 3a and 3b), only the irreversible oxidation of the latter was visible since the concentration of the co-reactant is 100 times larger than that of BTXI. In the corresponding ECL channel,

no ECL was detected before the oxidation of BTXI, confirming the necessity to form *in situ* $BTXI^{\bullet+}$and $TPA^{\bullet+}$ to initiate the sequence of steps leading to photon emission (eqs. 2, 5, 6, 7, and 4). To estimate the ECL yield, the same experiment was performed with $Ru(bpy)_3^{2+}$ as a standard ECL reference (see Figure S3a). Hence, and under similar conditions, the ECL yield of BTXI was estimated to be 13% of that of the $Ru(bpy)_3^{2+}$ reference. The ECL efficiency decreased to 6% for BTXI-DPA (Table 3). Note that ECL yields were calculated from at least four independent measurements. In all cases, the ECL signal was weighted by the current recorded during the corresponding LSV. A comparable series of experiments was performed by applying a negative potential sweep in the presence of BPO. These results are gathered in Figures 3c and 3d. One can see that the corresponding LSV curves show several reduction peaks, the first one being associated with the reduction of BPO at a potential of ~ [–0.4, –0.7 V] *vs.* Ag. Once again, the ECL emission starts only when the applied potential is more negative than the reduction potential of BTXI molecules. The ECL signal starts to rise at E = –1.4 V and –1.3 V for BTXI and BTXI-DPA, respectively. Compared to $Ru(bpy)_3^{2+}$(Figure S3b), ECL yields of 75% and 55% were calculated for BTXI and BTXI-DPA, respectively (Table 3). One can note that these ECL efficiency values should be interpreted with caution. Indeed, the current used for the normalization of the ECL signal is affected by many parameters such as the electrode surface state and is dominated by the co-reactant concentration, which is two orders of magnitude larger than the dye concentration. However, a qualitative comparison remains possible and is well-admitted in the field. BTXI appears to be more efficient via both co-reactant pathways despite a lower free enthalpy of the associated reactions. Again, in this case, the superior quantum yield of BTXI (*i.e.* 99%) seems a reasonable explanation to rationalize this difference of ECL yields since BTXI-DPA suffers from a lower $\boldsymbol{\phi_{PL}}$ value (33%).

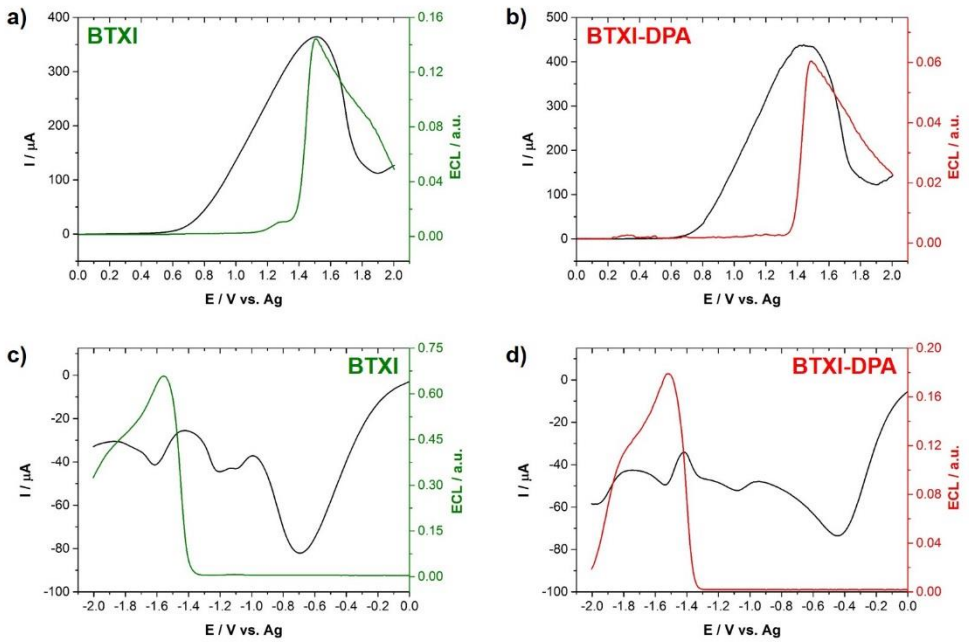

Figure 3. Linear sweep voltammograms (black curves) and corresponding ECL signals recorded in CH_3CN solution containing 1 mM of BTXI (green lines) or 1 mM of BTXI-DPA (red lines) in 0.1 M $TBAPF_6$. The ECL is promoted according to the co-reactant pathway by using either 0.1 M TPA (a,b) or 0.01 M BPO (c,d), respectively. A GC disk was used as working electrode and a silver-wire as pseudo-reference electrode. Scan rate: 0.1 V s^{-1}.

Finally, the ECL spectra were compared to the corresponding fluorescence spectra. To do so, ECL emission was directly collected by a remote spectrometer in combination with a homemade spectro-electrochemical cell. CH_3CN solutions containing 1 mM of dye, 100 mM of TPA, and 0.1 M of $TBAPF_6$ were used. The signal was accumulated for 30 seconds while a potential of 2.0 V *vs.* Ag pseudo-reference was applied to build up the corresponding ECL spectra. The ECL spectrum of BTXI is given in Figure 4a (solid line) with a broad band around 520-530 nm, corresponding to green light emission. By comparison, the fluorescence spectrum recorded at 10 µM (dashed line) features a maximum at λ = 510 nm and a narrower emission band. This 10 nm-red shift is not completely surprising since the spectra were collected with two different apparatus and at very different concentrations. Indeed, a concentration of 1 mM in dye affords a reasonable ECL signal but might cause a significant inner filter effect due to a partial re-absorption of the photons emitted, responsible for the observed shift. Nevertheless, we can conclude that the same excited state is reached by ECL and PL for this molecule. An ECL spectrum was similarly collected for BTXI-DPA revealing a slightly noisier signal with a maximum at 615 nm (Figure 4b, solid line). The corresponding PL spectrum (dashed line) has a large band with a maximum pointing at ~ 600 nm, confirming the emission in the red visible region. As for BTXI, the red shift observed between PL and ECL spectra collected for BTXI-DPA can be attributed to the large optical density of the concentrated solution necessary for ECL.

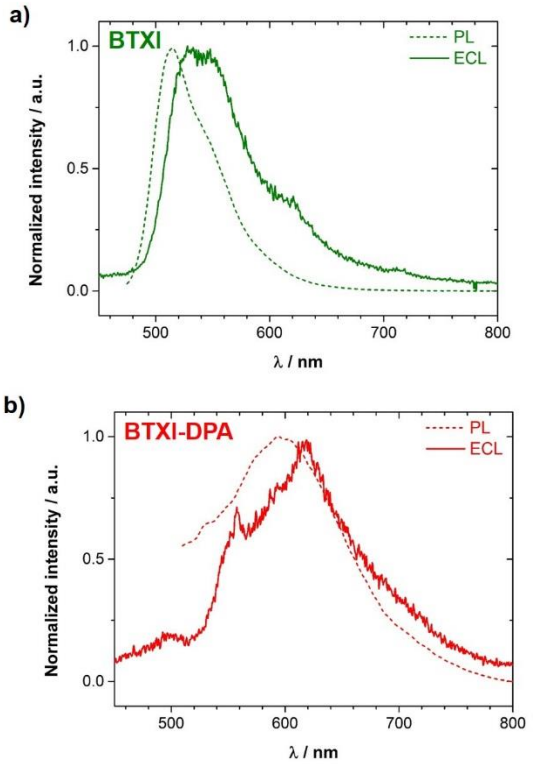

Figure 4. Representative photoluminescence (PL, dashed lines) and ECL (solid lines) spectra recorded in CH_3CN. The ECL spectra were recorded under electrochemical control by applying 2.0 V *vs.* Ag for 30 s with a solution containing 0.1 M $TBAPF_6$, 0.1 M TPA as co-reactant and 1 mM of BTXI (a) or 1 mM BTXI-DPA (b) dye. Fluorescence spectra were recorded in solutions that contained 10 μM of dye. $\lambda_{excitation}$ = 455 nm (a) and 490 nm (b), respectively.

Conclusion

To investigate a new potential class of ECL-active dyes, we report the successful use of the overlooked BTXI moiety as an ECL emitter. Herein, the bare BTXI structure was tested and compared to a diphenylamine functionalized analogue. BTXI is a green emitter with an almost quantitative PL quantum yield. However, conjugation with DPA resulted in red emission and reduced quantum efficiency. Both molecules were characterized by electrochemistry consistently revealing a pair of reversible reduction processes at potentials of ~ –1 V *vs.* Ag pseudo-reference and oxidations at +1.55 V or +1.35 V for BTXI and BTXI-DPA, respectively. A direct comparison between these typical potential values and the energy of the excited states of the dyes indicates that ECL generation should be possible. Consequently, several ECL mechanisms were considered and tested confirming the suitability of both dyes according to the annihilation pathway as well as two different co-reactant pathways. Hence, ECL was first generated by alternately pulsing the applied potential between the reduction and oxidation potentials in order to generate reactive species that can undergo a homogeneous redox reaction to populate the excited state of the dye. For both compounds, the oxidized form was found to limit the ECL capability and the presence of the DPA group appears to be slightly more effective. The use of sacrificial co-reactants to promote either an “oxidative-reduction” or a “reductive-oxidation” mechanism was also successful. With TPA, ECL yield values of 13% and 6% for BTXI and BTXI-DPA respectively were measured relative to a $Ru(bpy)_3^{2+}$ standard. On the other hand, the corresponding yields with BPO co-reactant were found to be of 75% and 55%, respectively. Finally, BTXI is a very promising ECL candidate since this cheap and accessible electroactive molecule can be readily activated via several different ECL pathways. Moreover, BTXI can be readily functionalized with a variety of chemical groups, making a large chemical diversity possible in order to fine-tune the corresponding physical properties, such as solubility, ECL potential, ECL wavelength, and beyond.

Experimental Section

Chemicals.

Benzothioxanthenes were synthetized at MOLTECH-Anjou Laboratory according to a previously described protocol.[42,45] Acetonitrile (CH_3CN, anhydrous, 99.8%) was purchased from Sigma-Aldrich. Tetra-*n*-butylammonium hexafluorophosphate ($TBAPF_6$, 98%) was purchased from Alfa Aesar. Tri-*n*-propylamine (TPA, ≥ 98%) and benzoyl peroxide (BPO, Luperox® A75FP, 75% remainder water) containing 25 wt. % of H_2O as stabilizer were purchased from Sigma Aldrich and used without further purification. Tris(2,2′-bipyridine) ruthenium(II) hexafluorophosphate ($Ru(bpy)_3^{2+}$, 97%) and ferrocene (98%) were also purchased from Sigma Aldrich.

Electrochemistry.
CV experiments were performed with a µ-Autolab (type III) potentiostat connected to a conventional three-electrode cell, consisting in a silver wire pseudo-reference electrode, a platinum-grid auxiliary electrode and a GC disk (3 mm in diameter) working electrode. Prior to measurements, the GC disk was polished with alumina slurry, rinsed thoroughly with Milli-Q water, sonicated in CH_3CN for 5 min. and dried with a N_2 stream. Analytical solutions containing 1 mM of redox probe were prepared with 0.1 M of $TBAPF_6$ as a supporting electrolyte. Data acquisition was performed with either GPES or NOVA softwares. CV was recorded with a step potential of 5 mV and at a scan rate of 0.1 V s^{-1}. CV of a ferrocene reference was characterized using the same experimental conditions. Under these conditions, the ferrocene/ferrocenium (Fc/Fc^+) redox couple displayed a formal potential value of 0.61 V *vs.* Ag.

Electrogenerated chemiluminescence.
ECL intensity was measured using a Hamamatsu photomultiplier tube (PMT) R5070A with a Hamamatsu C9525 high voltage power supply. The PMT detector was held at 750 V and placed at a constant distance of 5 mm in front of the GC working electrode. The output signal was amplified by a Keithley 6485 Picoammeter before acquisition *via* the second input channel of a PGSTAT30 potentiostat. The annihilation ECL pathway was studied at a concentration of 0.1 mM of redox probe whereas 100 mM of TPA or 10 mM of BPO were employed to investigate the co-reactant pathways in the presence of 1 mM of the redox probe. ECL spectra were recorded by using a Princeton Instruments Acton SpectraPro 2300i. The electrochemical cell was built with a glass slide at the bottom to collect *in-situ* the ECL signal. An optical fiber was connected to the device and placed in front of a transparent glass slide at close proximity to the working electrode. During a chronoamperometric experiments, a potential step of 2.0 V *vs.* Ag was applied by a potentiostat (µ-Autolab, type III) and the spectra were acquired during 30 s using a grating of 150.

Acknowledgements

A.L.D. acknowledges the University of Bordeaux for a PhD studentship. L.B. thanks the CNRS and the Department Science & Technology of the University of Bordeaux for funding (AAP 2017, project MICRO-REDOX). J.M.A.C. thanks the European Union's Horizon 2020 research and innovation program under Marie Sklodowska-Curie Grant agreement No.722651 (SEPOMO). C.C. thanks the ANR for the funding of the "BTXI-APOGEE" project (ANR-20-CE05-0029).

Keywords: Benzothioxanthene • luminophore • electro-chemiluminescence • annihilation • structure-activity relationship

[1] M. M. Richter, *Chem. Rev.* **2004**, *104*, 3003-3036.
[2] W. Miao, *Chem. Rev.* **2008**, *108*, 2506-2553.
[3] R. J. Forster, P. Bertoncello, T. E. Keyes, *Annu. Rev. Anal. Chem.* **2009**, *2*, 359-385.
[4] Z. Liu, W. Qi, G. Xu, *Chem. Soc. Rev.* **2015**, *44*, 3117-3142.
[5] A. Kapturkiewicz, *ChemElectroChem* **2017**, *4*, 1604-1638.
[6] L. Bouffier, N. Sojic, in *Chapter 1 Introduction and Overview of Electrogenerated Chemiluminescence*, The Royal Society of Chemistry, **2020**, pp.1-28.
[7] W. Zhao, H.-Y. Chen, J.-J. Xu, *Chem. Sci.* **2021**, *12*, 5720-5736.
[8] A. Zanut, A. Fiorani, S. Canola, T. Saito, N. Ziebart, S. Rapino, S. Rebeccani, A. Barbon, T. Irie, H.-P. Josel, F. Negri, M. Marcaccio, M. Windfuhr, K. Imai, G. Valenti, F. Paolucci, *Nat. Commun.* **2020**, *11*, 2668.
[9] W. Miao, L. Lu, in *Chapter 3 Efficient ECL Luminophores*, The Royal Society of Chemistry, **2020**, pp.59-91.
[10] M. W. Glasscott, J. E. Dick, *The Journal of Physical Chemistry Letters*, **2020**, *11*, 4803-4808.
[11] P. Dutta, D. Han, B. Goudeau, D. Jiang, D. Fang, N. Sojic, *Biosens. Bioelectron.* **2020**, *165*, 112372.
[12] M. W. Glasscott, S. Voci, P. J. Kauffmann, A. I. Chapoval, J. E. Dick, *Langmuir* **2021**, *37*, 2907-2912.
[13] H. Li, L. Bouffier, S. Arbault, A. Kuhn, C. F. Hogan, N. Sojic, *Electrochem. Commun.* **2017**, *77*, 10-13.
[14] T. Nobeshima, M. Nakakomi, K. Nakamura, N. Kobayashi, *Adv. Optic. Mater.* **2013**, *1*, 144-149.
[15] H. C. Moon, T. P. Lodge, C. D. Frisbie, *J. Am. Chem. Soc.* **2014**, *136*, 3705-3712.
[16] D.-K. Kwon, J.-M. Myoung, *Chem. Eng. J.* **2020**, *379*, 122347.
[17] M. Schmittel, Q. Shu, M. E. Cinar, *Dalton Trans.* **2012**, *41*, 6064-6068.
[18] K. N. Swanick, S. Ladouceur, E. Zysman-Colman, Z. Ding, *Angew. Chem. Int. Ed.* **2012**, *51*, 11079-11082.
[19] B. D. Stringer, L. M. Quan, P. J. Barnard, D. J. D. Wilson, C. F. Hogan, *Organometallics*, **2014**, *33*, 4860-4872.
[20] S. Voci, R. Duwald, S. Grass, D. J. Hayne, L. Bouffier, P. S. Francis, J. Lacour, N. Sojic, *Chem. Sci.* **2020**, *11*, 4508-4515.
[21] L. C. Soulsby, J. Agugiaro, D. J. D. Wilson, D. J. Hayne, E. H. Doeven, L. Chen, T. T. Pham, T. U. Connell, A. J. Driscoll, L. C. Henderson, P. S. Francis, *ChemElectroChem* **2020**, *7*, 1889-1896.
[22] M. Hesari, S. M. Barbon, V. N. Staroverov, Z. Ding, J. B. Gilroy, *Chem. Commun.* **2015**, *51*, 3766-3769.
[23] C. Adam, A. Wallabregue, H. Li, J. Gouin, R. Vanel, S. Grass, J. Bosson, L. Bouffier, J. Lacour, N. Sojic, *Chem. Eur. J.* **2015**, *21*, 19243-19249.
[24] F. Rizzo, F. Polo, G. Bottaro, S. Fantacci, S. Antonello, L. Armelao, S. Quici, F. Maran, *J. Am. Chem. Soc.* **2017**, *139*, 2060-2069.
[25] H. Li, R. Duwald, S. Pascal, S. Voci, C. Besnard, J. Bosson, L. Bouffier, J. Lacour, N. Sojic, *Chem. Commun.* **2020**, *56*, 9771-9774.
[26] Y. Koinuma, R. Ishimatsu, E. Kato, J. Mizuno, T. Kasahara, *Electrochem. Commun.* **2021**, *127*, 107047.

[27] C.-G. Niu, X.-Q. Gui, G.-M. Zeng, A.-L. Guan, P.-F. Gao, P.-Z. Qin, *Anal. Bioanal. Chem.* **2005**, *383*, 349-357.
[28] Z.-Z. Li, C.-G. Niu, G.-M. Zeng, Y.-G. Liu, P.-F. Gao, G.-H. Huang, Y.-A. Mao, *Sens. Actuators B Chem.* **2006**, *114*, 308-315.
[29] C.-G. Niu, A.-L. Guan, G.-M. Zeng, Y.-G. Liu, G.-H. Huang, P.-F. Gao, X.-Q. Gui, *Anal. Chim. Acta*, **2005**, *547*, 221-228.
[30] Z.-Z. Li, C.-G. Niu, G.-M. Zeng, P.-Z. Qin, *Chem. Lett.* **2009**, *38*, 698-699.
[31] M. Danko, Š. Chmela, P. Hrdlovič, *Polym. Degrad. Stab.* **2006**, *91*, 1045-1051.
[32] Š. Chmela, J. Kollár, L. Hrčková, *J. Photochem. Photobiol. A Chem.* **2015**, *307-308*, 123-130.
[33] M. Danko, P. Hrdlovič, Š. Chmela, *Polym. Degrad. Stab.* **2011**, *96*, 1955-1960.
[34] J. Kollár, Š. Chmela, P. Hrdlovič, *J. Photochem. Photobiol. A Chem.* **2013**, *270*, 28-36.
[35] F. Tronc, M. Li, J. Lu, M. A. Winnik, B. L. Kaul, J.-C. Graciet, *J. Polym. Sci. Pol. Chem.* **2003**, *41*, 766-778.
[36] Š. Chmela, L. Hrčková, *Eur. Polym. J.* **2009**, *45*, 2580-2586.
[37] P. Mao, X. Qian, H. Zhang, W. Yao, *Dyes and Pigments*, **2004**, *60*, 9-16.
[38] M. Ilčíková, M. Danko, M. Doroshenko, A. Best, M. Mrlík, K. Csomorová, M. Šlouf, D. Chorvát, K. Koynov, J. Mosnáček, *Eur. Polym. J.* **2016**, *79*, 187-197.
[39] Y. Sato, T. Ogata, S. Ichinosawa, Y. Murata, *Synth. Met.* **199**7, *91*, 103-107.
[40] P. Josse, S. Li, S. Dayneko, D. Joly, A. Labrunie, S. Dabos-Seignon, M. Allain, B. Siegler, R. Demadrille, G. C. Welch, C. Risko, P. Blanchard, C. Cabanetos, *J. Mater. Chem. C* **2018**, *6*, 761-766.
[41] A.-J. Payne, N. A. Rice, S. M. McAfee, S. Li, P. Josse, C. Cabanetos, C. Risko, B. H. Lessard, G. C. Welch, *ACS Appl. Energy Mater.* **2018**, *1*, 4906-4916.
[42] S. V. Dayneko, A. D. Hendsbee, J. R. Cann, C. Cabanetos, G. C. Welch, *New J. Chem.* **2019**, *43*, 10442-10448.
[43] J. M. Andrés Castán, C. Dalinot, S. Dayneko, L. Abad Galan, P. Simón Marqués, O. Alévêque, M. Allain, O. Maury, L. Favereau, P. Blanchard, G. C. Welch, C. Cabanetos, *Chem. Commun.* **2020**, *56*, 10131-10134.
[44] C. Dalinot, P. Simón Marqués, J. M. Andrés Castán, P. Josse, M. Allain, L. Abad Galán, C. Monnereau, O. Maury, P. Blanchard, C. Cabanetos, *European J. Org. Chem.* **2020**, *2020*, 2140-2145.
[45] J. M. Andrés Castán, L. Abad Galán, S. Li, C. Dalinot, P. Simón Marqués, M. Allain, C. Risko, C. Monnereau, O. Maury, P. Blanchard, C. Cabanetos, *New J. Chem.* **2020**, *44*, 900-905.
[46] P. Simón Marqués, J. M. Andrés Castán, L. A. Galan, M. Allain, O. Maury, T. Le Bahers, P. Blanchard, C. Cabanetos, *J. Org. Chem.* **2021**, *86*, 5901-5907.
[47] L. A. Galán, J. M. Andrés Castán, C. Dalinot, P. S. Marqués, P. Blanchard, O. Maury, C. Cabanetos, T. Le Bahers, C. Monnereau, *Phys. Chem. Chem. Phys.* **2020**, *22*, 12373-12381.
[48] L. A. Galán, J. M. Andrés Castán, C. Dalinot, P. S. Marqués, J. Galiana, P. Blanchard, C. Andraud, E. Dumont, O. Maury, C. Cabanetos, C. Monnereau, T. Le Bahers, *J. Phys. Chem. B*, **2021**, DOI: 10.1021/acs.jpcb.1c05082.
[49] C. Malacrida, A. H. Habibi, S. Gámez-Valenzuela, I. Lenko, P. S. Marqués, A. Labrunie, J. Grolleau, J. T. López Navarrete, M. C. Ruiz Delgado, C. Cabanetos, P. Blanchard, S. Ludwigs, *ChemElectroChem* **2019**, *6*, 4215-4228.
[50] W. Miao, J.-P. Choi, A. J. Bard, *J. Am. Chem. Soc.* **2002**, *124*, 14478-14485.
[51] H. Li, A. Wallabregue, C. Adam, G. M. Labrador, J. Bosson, L. Bouffier, J. Lacour, N. Sojic, *J. Phys. Chem. C* **2017**, *121*, 785-792.
[52] E. A. Chandross, F. I. Sonntag, *J. Am. Chem. Soc.* **1966**, *88*, 1089-1096.
[53] D. L. Akins, R. L. Birke, *Chem. Phys. Lett.* **1974**, *29*, 428-435.
[54] J.-P. Choi, A. Bard, *J. Electroanal. Chem.* **2004**, *573*, 215-225.